ISSN 2393-9850
GEM — Georgian Educational Mine
Interdisciplinary International Peer-Reviewed Research Journal
St. George's College Aruvithura, Kerala, India

Volume 3, Issue 1, 2023
Pages 23–33
gem.sgcaruvithura.ac.in

ORIGINAL RESEARCH ARTICLE

Snowman-Shaped Dielectric Resonator Antenna For Wireless Sensor Applications

Rosamma Sebastian[1,2], Anju P Mathews[3], Tony Joseph[4], Sumesh George[1,*]

[1]Research and Postgraduate Department of Physics, St. George's College, Aruvithura, Kerala, India
[2]Department of Electronics and Communication Engineering, Amal Jyothi College of Engineering, Kanjirappally, Kerala, India
[3]Department of Physics, St. Joseph's College, Moolamattom, Kerala, India
[4]Department of Physics, Govt. Victoria College, Palakkad, Kerala, India

[*]**Corresponding author:** Sumesh George, sumesh@sgcaruvithura.ac.in

Received: 22 October 2023 · **Revised:** 24 November 2023 · **Accepted:** 15 December 2023 · **Published:** 19 December 2023

Keywords: Dielectric Ring Resonator Antenna; HDRR; Impedance bandwidth; UWB

Abstract

This article proposes a novel composite Hybrid Dielectric Ring Resonator (HDRR) antenna with a low-profile wideband monopole configuration. A new snowman-like dielectric resonator antenna (DRA) structure is presented, comprising a central monopole and three dielectric blocks. Ansoft HFSS simulation software was used to optimize the design. The current study discusses the impact of various parameters, including size and dielectric constant, on the antenna's bandwidth and gain. By carefully altering the dimensions and the dielectric constant of the material of the blocks, and utilizing iterative simulations and analysis, a novel-designed HDRR with reasonably high bandwidth and gain is created. The proposed snowman-inspired structure exhibits a promising maximum impedance percentage bandwidth of 135% in the frequency band 5.07–27.12 GHz and a peak gain of 11.49 dB at 5.66 GHz. The optimized structure of the new design employs a material with a dielectric constant of 8 and has been verified in another simulation software, CST. The proposed antenna can be used for industrial automation, such as wireless sensor networks and machine-to-machine communication.

1. INTRODUCTION

Next-generation communication systems require capacity and performance upgrades via advanced frequency bands and antenna networks. High data speeds of terabits per second (Tbps) require migration to higher frequency bands [Rappaport et al., 2017]. Increasing bandwidth and gain is the most effective way to satisfy future demand. However, shorter wavelengths in higher frequency bands cause path loss during short-distance transmission [Feng et al., 2016]. To tackle these challenges, other types of antennas such as patch antennas, lens antennas, and array antennas were developed [Santillán-Haro et al., 2018]. Dielectric resonator antennas (DRAs) are a promising substitute due to their unique properties, such as negligible conduction loss, high radiation efficiency, large bandwidth, small size, low profile, excellent design flexibility, and more. Long et al. created the DRA in 1982 [Long et al., 1983], by substituting the microstrip antenna's radiating metallic patch with a high-permittivity dielectric material to reduce metal-induced losses. The DRA is easy to construct and feed through various coupling techniques, such as a coaxial probe, slot line, strip line, microstrip line, or coupled aperture. Compared to the patch antenna, there are no losses from surface waves because the DRA element is directly positioned on the ground plane, and radiation occurs from its entire surface [Mongia and Ittipiboon, 1997].

Several shapes, including rectangular, cylindrical, triangular, hemispherical, and composite, are currently available in DRA structures. Cylinder-shaped DRAs have radius and height as their design parameters and are easier to design [Drossos et al., 1999]. The analysis of open literature indicates that improving bandwidth and gain is the primary focus of DRA research [Smida, 2021]. To increase the gain, uniaxial anisotropic materials are incorporated into DRAs [Fakhte and Oraizi, 2016]. To enhance the impedance bandwidth of the antenna, several methods have been proposed in the published literature, including multilayer or stacked DRAs of different dielectric materials [Pan and Zheng, 2016, Kumar et al., 2019], rotated-stairs configurations [Wang and Wong, 2015], and sandwiched structures of two ceramic sheets of high and low permittivity [Sun et al., 2018]. Some of the previously reported wideband hybrid DRAs are summarized in Table 1.

Inspired by a set of literature [Guha et al., 2012, Sharma and Biswas, 2017, Lin and Wu, 2022], a small-scale 3D UWB antenna design has been developed using a hybrid antenna technique. The hybrid antenna combines a quarter-wave monopole antenna with stacked conical, cylindrical, and spherical dielectric ring resonators (DRRs). This new construction improves impedance bandwidth while preserving monopole-type radiation across the whole band. The structure achieves a 135% impedance bandwidth and a maximum gain of 11.49 dB at 5.66 GHz.

2. ANTENNA DESIGN

Conical, cylindrical, and spherical DRAs have been investigated by various research groups [Zhong et al., 2015, Dey and Hesselbarth, 2020, Guha et al., 2022]. The present work is a combination of all three shapes. The cross-sectional and isometric view of the proposed structure of the hybrid DRR with a monopole feed is shown in Figure 1. This investigation of the proposed structure started with design parameters as used in [Guha et al., 2012]. Figure 2 shows the methodology for achieving the final proposed structure. The hybrid DRR antenna's dimensions were studied extensively to optimize its bandwidth. The framework is shaped like a composite, with a conical bottom, a cylindrical middle, and a spherical top. The construction itself resembles a snowman. The core of the proposed structure is a monopole ($l = 11$ mm, $r = 0.65$ mm) with a 50 Ω coaxial-probe feed, which determines the lower end of the frequency band and acts as the feed. A cylindrical portion of radius $a = 1.5$ mm in all three structures is cut out to accommodate the monopole. The proposed antenna is located in the middle of the ground plane with dimensions equal to 50×50 mm. The cut-out radius a is a determining factor for the mutual coupling between the monopole and the DRA.

Table 1. Previously documented hybrid DRA structures.

Structure Investigated	Year	Frequency Range
Annular ring DR excited by electric monopole [Lapierre et al., 2005]	2005	6–18 GHz
Inverted conical DRA fed with monopole [Jazi and Denidni, 2008]	2008	2–7 GHz
Pawn-shaped DRR fed by hybrid monopole [Guha et al., 2009]	2009	5.5–23 GHz
Rectangular DRA with tapered strip excitation [Khalily et al., 2011]	2011	2.13–6.08 GHz
High gain broadband CDRA [Wang et al., 2013]	2013	5.4–6.8 GHz
Cup-shaped hemispherical DRA [Mukherjee et al., 2013]	2013	1.8–3.7 GHz
Two-segment ring DRA [Sharma and Gangwar, 2016]	2016	3.45–10.9 GHz
Mushroom-shaped DRA [Guha et al., 2017]	2017	4.9–25 GHz
Circularly polarized fractal HDRA [Shabya et al., 2019]	2019	3.3–5.9 GHz

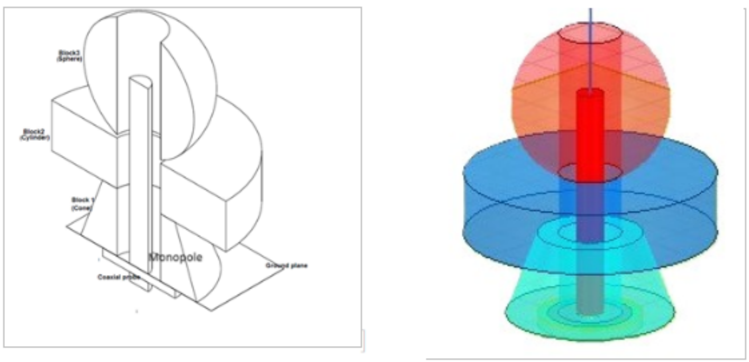

Figure 1. Cross-section and Isometric view of the proposed structure of the Hybrid DRR

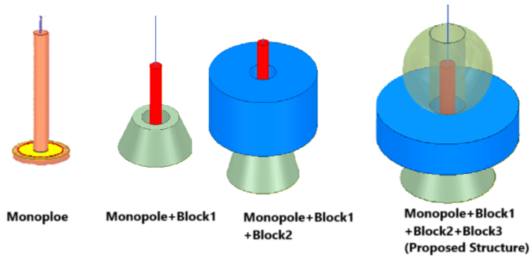

Figure 2. Proposed Antenna Evolution step by step

All parameter values were fixed through parametric analysis performed in Ansoft HFSS. The monopole height was optimized to function as a quarter-wave antenna and to excite the DRR in the TM_{01} mode, resulting in closely spaced multiple resonances across a wide bandwidth. The dielectric constant of the proposed antenna was also optimized for maximum bandwidth through iterative HFSS simulations. The optimized antenna parameters and corresponding percentage bandwidth for the designs are summarized in Table 2.

Table 2. Optimized geometric parameters and bandwidth performance of the proposed snowman-inspired hybrid DRR antenna.

Structure	**Height (mm)**	**Radius (mm)**	**Notes**
Monopole feed	11.0	0.65	Quarter-wave at lower band edge
Conical DRR section	4.0	$U_r = 2.5$, $L_r = 4.0$	U_r: upper radius; L_r: lower radius
Cylindrical DRR section	3.0	6.0	Uniform cross-section
Spherical DRR section	–	3.8	Radius of spherical cap
Common Parameters			
Cut-out radius (all sections)	$a = 1.5$ mm (central monopole accommodation)		
Dielectric constant (ε_r)	8.0		
Ground plane dimensions	50×50 mm		
Performance Metrics			
Lower cutoff frequency (f_l)	5.07 GHz		
Upper cutoff frequency (f_u)	27.12 GHz		
Impedance bandwidth ($f_u - f_l$)	22.05 GHz		
Percentage bandwidth	135%		
Peak gain	11.49 dB at 5.66 GHz		

3. RESULTS AND DISCUSSION

The input impedance of the proposed hybrid DRR is shown in Figure 3. The real part represents the resistive component of the impedance. Its values remain close to 50 Ω across the operating band, indicating minimal energy loss as heat and enabling maximum power transfer with low reflection. The imaginary part displays the reactive components, and its zero-crossing points correspond to the resonant frequencies of the antenna. The impedance curve of the proposed structure exhibits an excellent match over a broad frequency range, confirming the wide bandwidth performance.

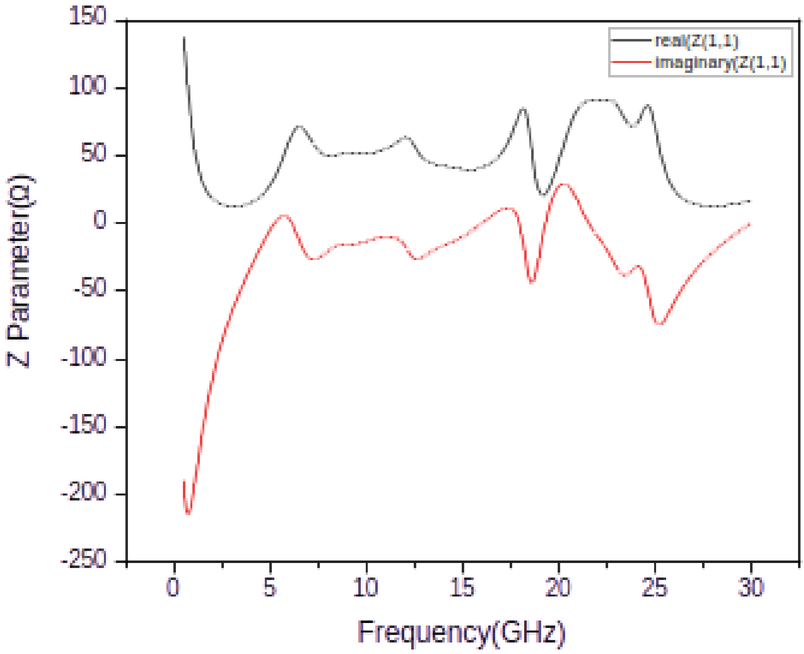

Figure 3. Simulated input impedance of the proposed hybrid DRR antenna: real (resistive) and imaginary (reactive) components versus frequency.

The proposed hybrid structure was developed in three iterative design stages: (i) a bare monopole feed, (ii) addition of a conical DRR around the monopole (lower radius $L_r = 4.0$ mm, upper radius $U_r = 2.5$ mm, height = 4.0 mm), and (iii) stacking of cylindrical and spherical DRR sections. The monopole alone exhibits dual-band resonances at 6.32 GHz and 19.38 GHz. However, the introduction of the conical DRR significantly modifies the resonant behavior, as shown in Figure 4.

To systematically study the impact of dielectric block geometry on resonant behavior, cylindrical and spherical sections were sequentially added to the conical DRR. The reflection coefficient (S_{11}) characteristics at each stage are presented in Figure 5. Stacking different dielectric blocks enhances the antenna's radiating properties by introducing additional resonant modes and improving impedance matching.

The final proposed structure—comprising a conical base, cylindrical middle, and spherical top (resembling a snowman)—exhibits three distinct resonances at 5.52 GHz, 10.9 GHz, and 16.58 GHz. As evident from Figure 5, $S_{11} < -10$ dB over the frequency range 4.78–18.27 GHz, corresponding to an impedance bandwidth ratio exceeding 3.8:1, or approximately 117% fractional bandwidth.

Quantitative bandwidth progression across design stages is summarized as follows:

- Monopole alone: dual-band centered at 6.32 GHz and 19.38 GHz
- Monopole + conical DRR: 46% bandwidth
- Monopole + conical + cylindrical DRR: 77% bandwidth
- Full snowman structure (monopole + cone + cylinder + sphere): 117% bandwidth

These results confirm that the monopole serves as an efficient feed mechanism for the stacked DRR blocks, while the dielectric resonators collectively broaden the operational bandwidth through mode coupling and impedance transformation [Guha et al., 2012, Sharma and Biswas, 2017].

All simulations above employed dielectric blocks with $\varepsilon_r = 10$. To further optimize material selection, the dielectric constant was parametrically varied. Figure 6 illustrates the return loss characteristics for the snowman structure with $\varepsilon_r = 8$ across all blocks. This optimization yields a significantly improved impedance bandwidth of 135% (5.07–27.12 GHz).

Figure 7 presents the reflection coefficient of the fully optimized snowman-structured antenna

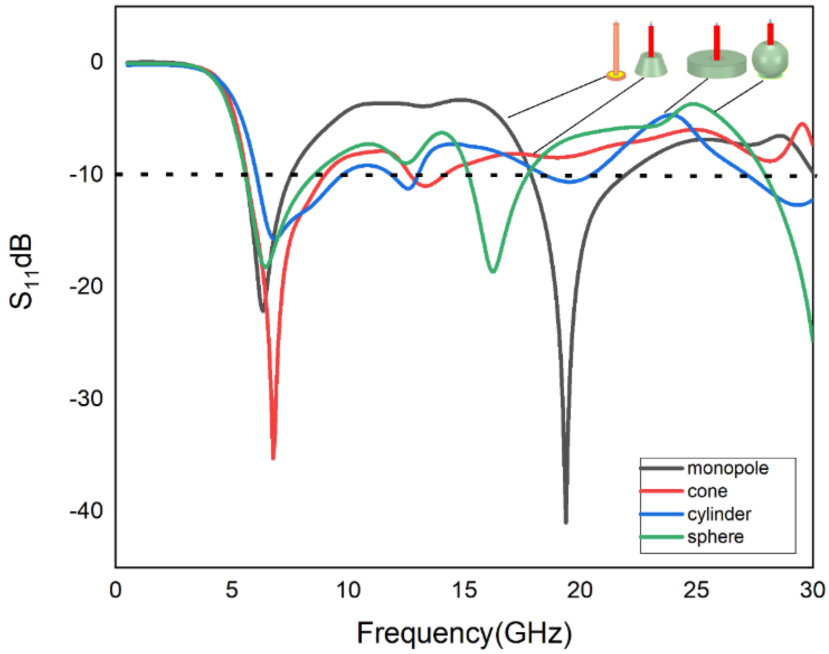

Figure 4. Reflection coefficient (S_{11}) characteristics of the monopole-loaded conical DRR block.

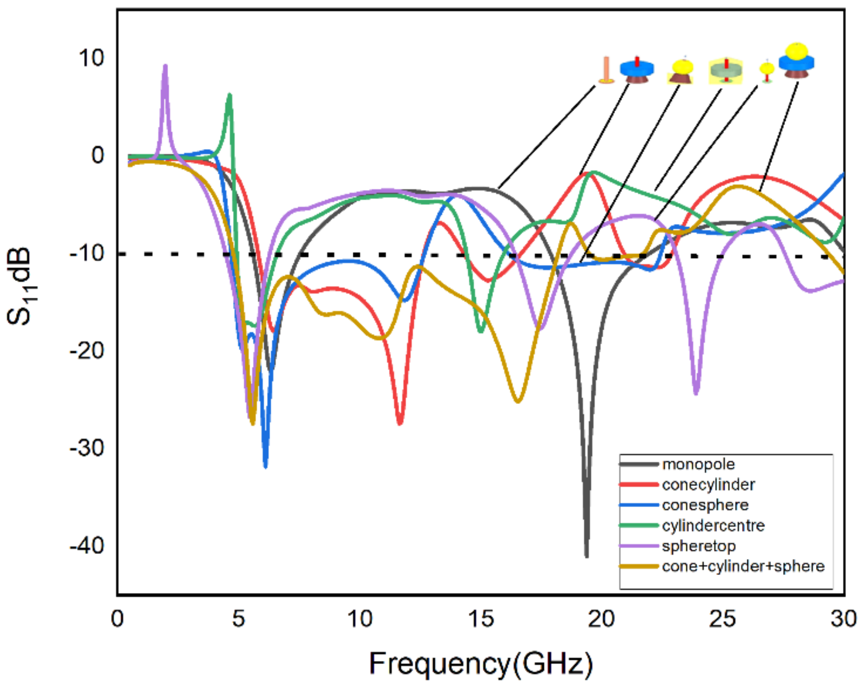

Figure 5. Reflection coefficient (S_{11}) characteristics of the hybrid DRR with sequentially stacked dielectric blocks: monopole only, monopole+cone, monopole+cone+cylinder, and full snowman structure.

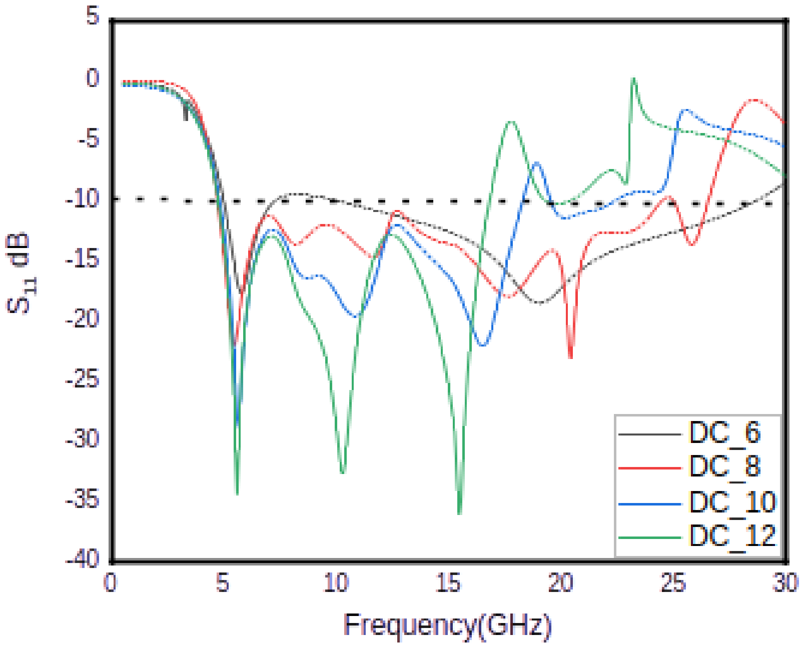

Figure 6. Reflection coefficient (S_{11}) characteristics of the snowman-structured DRR for varying dielectric constants (ε_r). Optimal bandwidth achieved at $\varepsilon_r = 8$.

($\varepsilon_r = 8$) simulated in Ansoft HFSS. To validate design reproducibility, the structure was independently simulated in Computer Simulation Technology (CST) Microwave Studio. Both simulators produced nearly identical S_{11} responses, confirming the feasibility and robustness of the proposed design [Lin and Wu, 2022].

Figures 8(a) and 8(b) display the 3D gain patterns of the optimized antenna at 5.66 GHz and 20.7 GHz, respectively. In the H-plane, the peak gain reaches 11.49 dB at 5.66 GHz, directed at approximately $-125°$ from broadside. Similarly, a peak gain of 9.96 dB is observed at 20.7 GHz in the E-plane at an angle of $-28°$. These results confirm stable, high-gain radiation across the ultra-wideband operating range.

Figures 9(a) and 9(b) present the simulated 2D radiation patterns at 5.66 GHz and 20.7 GHz. Adequate isolation between co-polarized and cross-polarized components is maintained across both frequencies, satisfying a key requirement for efficient antenna operation in polarization-sensitive applications [Zhong et al., 2015].

Figure 10 illustrates the electric field and surface current distributions of the optimized snowman-shaped antenna and monopole feed at two representative resonant frequencies: (a) 5.66 GHz and (b) 20.7 GHz. Strong field confinement within the dielectric blocks at lower frequencies transitions to more distributed currents at higher frequencies, confirming the multi-mode excitation mechanism responsible for the ultra-wideband performance.

To meet the evolving requirements of 5G and beyond-5G communication systems, continued research in dielectric resonator antenna design is essential to develop compact, high-gain, ultra-wideband solutions [Rappaport et al., 2017, Dey and Hesselbarth, 2020]. In this context, the proposed snowman-inspired hybrid DRR structure presents a promising candidate for applications in wireless sensor networks, machine-to-machine communication, and industrial automation systems requiring robust wideband performance.

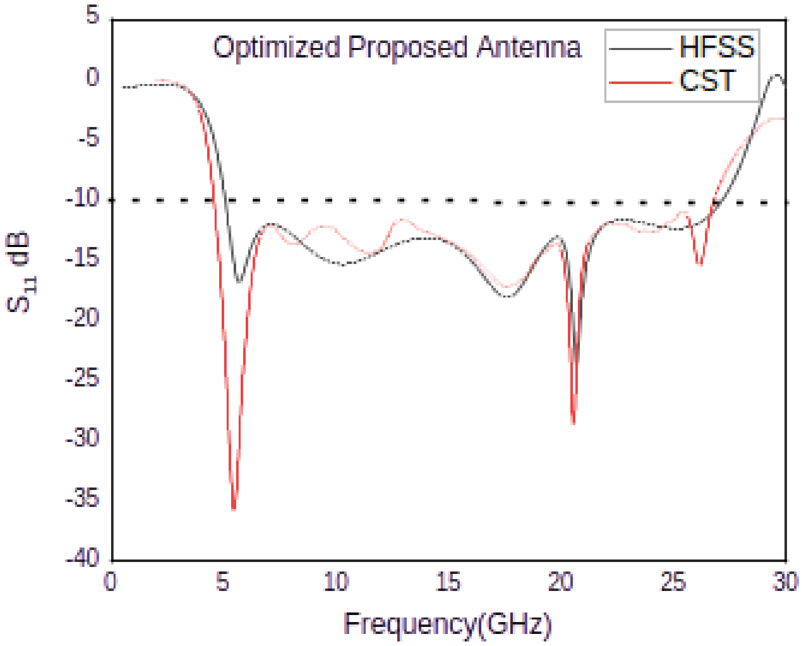

Figure 7. Comparison of reflection coefficient (S_{11}) characteristics for the optimized DRR ($\varepsilon_r = 8$) simulated in HFSS and CST, demonstrating cross-platform validation.

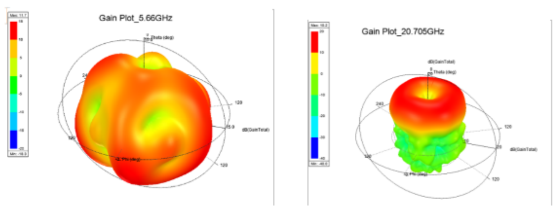

Figure 8. 3D polar plots of gain for the optimized hybrid DRR antenna at (a) 5.66 GHz and (b) 20.7 GHz.

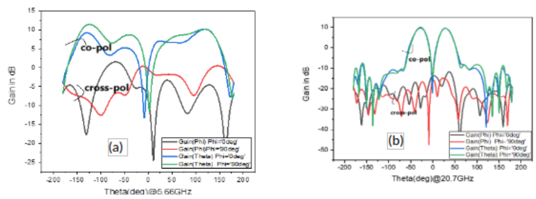

Figure 9. Simulated radiation patterns of the optimized hybrid DRR antenna: (a) at 5.66 GHz and (b) at 20.7 GHz, showing co-polar and cross-polar components in E- and H-planes.

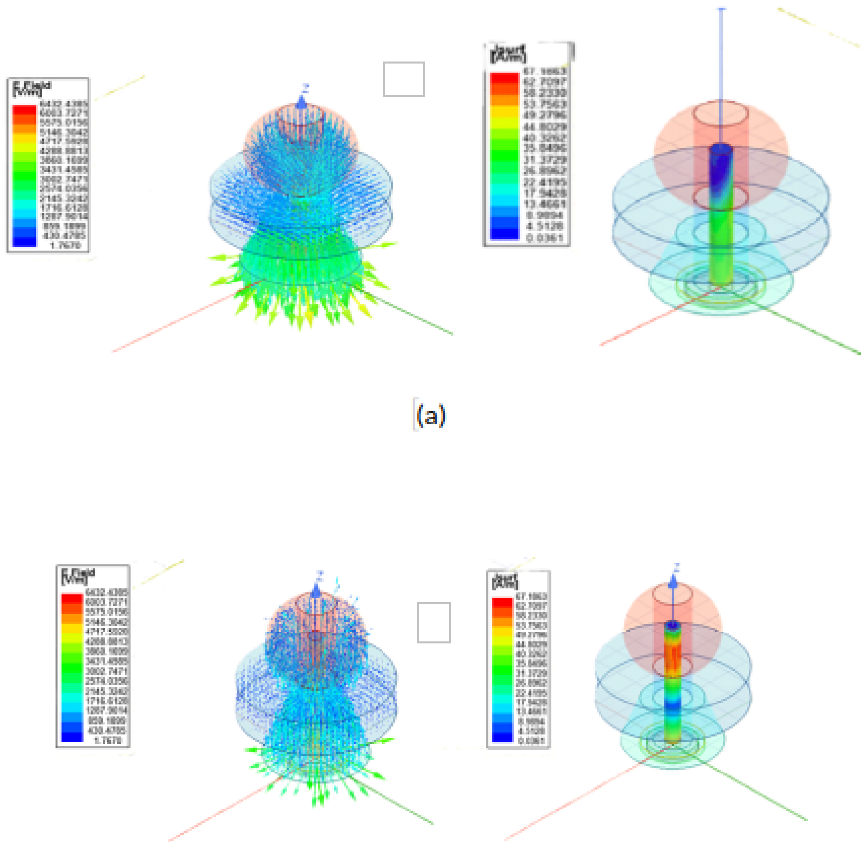

Figure 10. Electric field and surface current distributions in the optimized hybrid DRR antenna and monopole feed at resonant frequencies: (a) 5.66 GHz and (b) 20.7 GHz.

4. CONCLUSION

The design of a novel wideband, high-gain dielectric resonator antenna (DRA) featuring a snowman-inspired structure is proposed. The configuration comprises a hybrid dielectric ring resonator (DRR) with monopole-loaded DRA blocks. The dielectric blocks surrounding the central monopole are conical, cylindrical, and spherical, collectively resembling a snowman. Full-wave simulations demonstrate a peak gain of 11.49 dB at 5.66 GHz, with an impedance bandwidth of 135% spanning 5.07–27.12 GHz. The results were independently validated using Computer Simulation Technology (CST) Microwave Studio, confirming the design's robustness and reproducibility. Furthermore, the antenna maintains consistent radiation patterns and low cross-polarization levels across its operational frequency range. Owing to its ultra-wideband performance, high gain, and compact profile, the proposed topology is well-suited for next-generation communication applications, including 5G networks, satellite communications, radar and navigation systems, and military wireless links.

REFERENCES

U. Dey and J. Hesselbarth. *IEEE Antennas and Wireless Propagation Letters*, 19:1380–1384, 2020.

G. Drossos, Z. Wu, and L. E. Davis. *Microwave and Optical Technology Letters*, 20:36, 1999.

S. Fakhte and H. Oraizi. *Electronics Letters*, 52:1579–1581, 2016.

W. Feng, Y. Li, D. Jin, L. Su, and S. Chen. *Sensors*, 16:892, 2016.

D. Guha, B. Gupta, and Y. M. M. Antar. *IEEE Antennas and Wireless Propagation Letters*, 8: 1178–1181, 2009.

D. Guha, B. Gupta, and Y. M. M. Antar. *IEEE Transactions on Antennas and Propagation*, 60: 393–398, 2012.

D. Guha, D. Ganguly, S. George, C. Kumar, M. Sebastian, and Y. M. M. Antar. *IEEE Antennas and Propagation Magazine*, 59:139–152, 2017.

D. Guha, C. Sarkar, and Y. M. M. Antar. In *Proceedings of the 2022 IEEE International Symposium on Antennas and Propagation and USNC-URSI Radio Science Meeting (AP-S/URSI)*, pages 5–8, 2022.

M. N. Jazi and T. A. Denidni. In *Proceedings of the IEEE Antennas and Propagation Society International Symposium*, pages 1–4, 2008.

M. Khalily, M. K. A. Rahim, and A. A. Kishk. *IEEE Antennas and Wireless Propagation Letters*, 10: 393–396, 2011.

G. Kumar, M. Singh, S. Ahlawat, and R. S. Yaduvanshi. *Wireless Personal Communications*, 109: 1661–1675, 2019.

M. Lapierre, Y. M. M. Antar, A. Ittipiboon, and A. Petosa. *IEEE Microwave and Wireless Components Letters*, 15:7–9, 2005.

K. Z. Lin and T. T. Wu. *AEU – International Journal of Electronics and Communications*, 146: 154121, 2022.

S. A. Long, M. W. McAllister, and L. Shen. *IEEE Transactions on Antennas and Propagation*, 31: 406, 1983.

R. K. Mongia and A. Ittipiboon. *IEEE Transactions on Antennas and Propagation*, 45:1348, 1997.

B. Mukherjee, P. Patel, and J. Mukherjee. *IEEE Antennas and Wireless Propagation Letters*, 12: 1240–1243, 2013.

Y. M. Pan and S. Y. Zheng. *IEEE Antennas and Wireless Propagation Letters*, 15:68–71, 2016.

T. S. Rappaport, Y. Xing, G. R. MacCartney, A. F. Molisch, E. Mellios, and J. Zhang. *IEEE Transactions on Antennas and Propagation*, 65:6213, 2017.

D. Santillán-Haro, E. Antonino-Daviu, D. Sánchez-Escuderos, and M. Ferrando-Bataller. In *IEEE International Symposium on Antennas and Propagation & USNC/URSI National Radio Science Meeting*, page 1111, 2018.

G. Shabya, K. Vinay, C. Monika, and M. Biswajeet. *Frequenz*, 73:227–234, 2019.

A. Sharma and A. Biswas. *IET Microwaves, Antennas & Propagation*, 11:496–502, 2017.

A. Sharma and R. K. Gangwar. *International Journal of RF and Microwave Computer-Aided Engineering*, 26:47–53, 2016.

A. Smida. *Computers, Materials & Continua*, 71:1613–1625, 2021.

W. Sun, W. Yang, H. Tang, P. Chu, and J. Chen. *The Journal of Engineering*, pages 336–340, 2018.

K. X. Wang and H. Wong. *IEEE Antennas and Wireless Propagation Letters*, 14:787–790, 2015.

Y.-F. Wang, T. A. Denidni, Q.-S. Zeng, and G. Wei. *Electronics Letters*, 49:1506–1508, 2013.

L. Zhong, J. S. Hong, and H. C. Zhou. *IEEE Antennas and Wireless Propagation Letters*, 15: 1253–1256, 2015.